Eur. J. Mineral.
2017, **29**, 701–712
Published online 28 February 2017

**Special issue dedicated to Zdeněk Johan**

# Heptasartorite, $Tl_7Pb_{22}As_{55}S_{108}$, enneasartorite, $Tl_6Pb_{32}As_{70}S_{140}$ and hendekasartorite, $Tl_2Pb_{48}As_{82}S_{172}$, three members of the anion-omission series of 'sartorites' from the Lengenbach quarry at Binntal, Wallis, Switzerland

DAN TOPA[1,*], EMIL MAKOVICKY[2], BERTHOLD STOEGER[3] and CHRIS STANLEY[4]

[1] Naturhistorisches Museum, Burgring 7, 1010 Wien, Austria
*Corresponding author, e-mail: dan.topa@nhm-wien.ac.at
[2] Department of Geoscience and Resource Management, University of Copenhagen, Østervoldgade 10, 1350 Copenhagen K, Denmark
[3] Technische Universität Wien, Karlsplatz 13, 1040 Wien, Österreich
[4] Natural History Museum, Cromwell Road, London SW7 5BD, United Kingdom

**Abstract:** Detailed electron-microprobe investigations and crystal-structure determinations established that 'sartorite' represents a group of distinct mineral species, each with unique chemistry and crystal structure. These manifest themselves as the 7-, 9- and 11-fold $P2_1/c$ superstructures of the basic 4.2 Å substructure. Heptasartorite is $Tl_7Pb_{22}As_{55}S_{108}$ [based on 192 atoms per formula unit (*apfu*), 84Me + 108S] with $a = 29.269(2)$, $b = 7.8768(5)$, $c = 20.128(2)$ Å, $\beta = 102.065(2)°$ and unit-cell volume $V = 4537.8$ Å$^3$; enneasartorite is $Tl_6Pb_{32}As_{70}S_{140}$ (based on 248 *apfu*, 108Me + 140S) with $a = 37.612(6)$, $b = 7.8777(12)$, $c = 20.071(3)$ Å, $\beta = 101.930(2)°$ and $V = 5818.6(15)$ Å$^3$; hendekasartorite is $Tl_2Pb_{48}As_{82}S_{172}$ (based on 304 *apfu*, 132Me + 172S) (empirical $\Sigma$Me = 132.48) with $a = 31.806(5)$, $b = 7.889(12)$, $c = 28.556(4)$ Å and $\beta = 99.034(2)°$ with $V = 7076.4(15)$ Å$^3$. Physical and optical properties (grey with metallic lustre, in polished section white with visible bireflectance, red internal reflections; reflectance curves span 28.7–42.5%; Mohs hardness 3–3½) of these phases are very similar so that chemical analysis and/or single-crystal X-ray diffraction is needed to distinguish them. A brief description of complicated $As_mS_n$ crank-shaft chains in the walls of double-ribbons which form the As-based slabs of these structures is given. The three new mineral species differ in their structures by 4.2 Å modular increments, not just by cation substitutions. They represent anion-omission derivatives of the 'ideal' $PbAs_2S_4$ composition with an important role for thallium in charge compensation. The described minerals belong to the late sulfide phases in the Pb–Tl–Ag–As deposit of Lengenbach, Wallis, Switzerland.

**Key-words:** heptasartorite; enneasartorite; hendekasartorite; sartorite homologous series; anion-omission series; Pb–As sulfosalts; thallium substitution.

## 1. Introduction

The name sartorite was proposed by vom Rath (1864) in honour of Sartorius Waltershausen, a German mineralogist, to replace the name scleroclase of a mineral described by Waltershausen himself (1857; in Palache *et al.*, 1944) from the Lengenbach deposit, Binntal (Valais, Switzerland). The classical investigations of the mineral were supplemented by a crystal structure determination by Iitaka & Nowacki (1961), who proposed $PbAs_2S_4$ as formula for ideal sartorite. This determination, however, was performed on a substructure because it was already known that sartorite displayed faint superstructure on single-crystal X-ray diffraction photographs, which was estimated as a 20-tuple of the fundamental 4.2-Å period by Bannister *et al.* (1939) and Berry (1940), and as a 11-tuple by Nowacki *et al.* (1961); the 19.6-Å period was found to be tripled although Berry (1940) found it quadrupled.

Iitaka & Nowacki (1961) solved and refined the sartorite structure *on a subcell level* with the monoclinic space group $P2_1/n$, $a = 19.62$, $b = 7.89$, $c = 4.19$ Å, $\alpha = \beta = \gamma = 90°$, and Nowacki *et al.* (1961) stated that the true cell of sartorite is a commensurate superstructure with $3 \times a = 58.8$, $b = 7.89$, $11 \times c = 46.1$ Å and space group $P2_1/n$, but were not able to resolve it. Nowacki & Bahezre (1963) state, however, that the $3a \times b \times 11c$ true cell is not always present, and satellite reflections may occur instead in the X-ray diffraction photographs. Electron-diffraction studies on Lengenbach sartorite showed satellite reflections that were generally incommensurate with respect to the subcell $a = 19.62$, $b = 7.89$, $c = 4.19$ Å, $\beta = 90°$ and space group $P2_1/n$ (Pring *et al.*, 1993). From electron-diffraction data on unspecified Lengenbach sartorite, Pring (2001) gives a modulation vector 6/13(1 0 1)* for the same lattice.

DOI: 10.1127/ejm/2017/0029-2634
0935-1221/17/0029-2634 $ 5.40

Data on the true symmetry of sartorite varied widely, and this situation was only aggravated further by the results of Laroussi *et al.* (1989) who, in a detailed microprobe investigation of Lengenbach material, did not find a phase corresponding to the ideal sartorite, $PbAs_2S_4$, as defined by Iitaka & Nowacki (1961) on the basis of the substructure determination. Furthermore, for a long time, it was believed that sartorite is a pure Pb–As–S mineral. Nowacki & Bahezre (1963), Laroussi *et al.* (1989) and Berlepsch *et al.* (2003) have shown, however, that sartorite can contain variable amounts of thallium (from 2.6 to 6.5 wt% Tl, respectively).

The first hint of an explanation for this strange behaviour was in the results that Berlepsch *et al.* (2003) obtained on 'sartorite with a nine-fold superstructure'. Berlepsch *et al.* (2003) solved and refined a commensurate nine-fold sartorite superstructure with space group $P2_1/c$; $a = 37.71(2)$, $b = 7.898(3)$, $c = 20.106(8)$ Å, $\beta = 101.993(7)°$. The refined formula $Tl_{1.5}Pb_8As_{17.5}S_{35}$, with one-ordered sulfur vacancy, compares very well with the empirical formula $Tl_{1.4}Pb_{8.2}As_{17.5}Sb_{0.5}S_{35}$ obtained from electron-microprobe analyses. It has a high Tl content, up to 6.5 wt%. These authors suggest that the incorporation of substantial amounts of $Tl^+$ into $PbAs_2S_4$ is essential for the type and periodicity of superstructures in sartorite.

It might be worth mentioning that the mixed arsenic-antimony $N = 3$ sartorite homologues, twinnite $Pb_{0.8}Tl_{0.1}Sb_{1.3}As_{0.8}S_4$, space group $P2_1/n$ (Makovicky & Topa, 2012) and guettardite, $PbAsSbS_4$, space group $P2_1/c$ (Makovicky *et al.*, 2012), have simple 8.5–8.6 Å periods without modulation. The greater length of Sb–S bonds and other crystal–chemical properties of antimony eliminate the need for complicated superstructures which are present in arsenic-based $N = 3$ structures.

Based on fundamental structural properties, including the structure determinations by the Nowacki group (publications in the years 1961–1970) and Le Bihan (1962), Makovicky (1985) defined a *sartorite homologous series* of Pb–As and Pb–As–Sb sulfosalts with a set of common structural features and principles, and with sartorite as its lowermost member. As the number of phases belonging to this series, composed of phases with 3- and 4-coordination polyhedra broad ribbons found alone or in various quantitative and qualitative combinations, has been growing steadily, the definition of the series – based on the most fundamental principles – persisted well through all these incremental changes in its contents and was helpful in the ongoing research.

Our recent extensive study clarified the chemistry and crystal structure of various 'sartorite' specimens and revealed that we do not deal with varieties of one mineral species but with a group of closely related but structurally and chemically distinct minerals. The elucidation of the fine structure of the 'sartorite' species is one more refinement of the sartorite homologous series and the new minerals derived from the original 'sartorite' form a series of *anion-omission derivatives* (AOD) within the $N = 3$ homologues. We are describing here the first three commensurate members of the AOD-family: heptasartorite, enneasartorite and hendekasartorite.

*Heptasartorite* with a seven-fold superstructure based on the 4.2 Å subcell is so far the lowermost member of this omission series. The mineral and the mineral name were approved by the IMA-CNMNC (IMA 2015-073). *Enneasartorite* with nine-fold superstructure has the IMA 2015-074 approval and replaces '9-fold sartorite' of Berlepsch *et al.* (2003); the *hendekasartorite* with eleven-fold superstructure was approved under IMA 2015-075. Type materials are deposited in the reference collection of the Naturhistorisches Museum Wien, Austria, with catalogue numbers N 9859, N 9860 and N 9861, respectively.

The '9-fold sartorite' of Berlepsch *et al.* (2003) is the only phase that was properly described before the present study. At the time of its publication, it was believed to be an accidental 'lock-in phase', and consequently, there was no attempt to make a new mineral out of it. The present study confirms the wide existence of that phase and allowed us to transform it into a new mineral and also confirms all predictions about the sartorite family and the rules that govern it. Description of other species of the sulfur-omission series, with periodicity imperfections expressed as *non-commensurate* structures, will follow. When concerned with more than one species, we shall refer to 'M-sartorites' where M stands for hepta-, ennea- and hendeka (7, 9 and 11), or to AOD.

## 2. Occurrence

All three minerals occur at the Lengenbach deposit, Binntal (Valais, Switzerland), in a dolomite gangue. Recent detailed general descriptions of the locality are given by Graeser *et al.* (2008) and Roth *et al.* (2014). The Lengenbach deposit, as the type locality for almost 40 new mineral species (of which 24 are thallium-based minerals) is the most prolific locality worldwide for sulfosalts and sulfide minerals. The last new Lengenbach mineral descriptions are provided by Bindi *et al.* (2014, 2015) and Biagioni *et al.* (2016) concerning philrothite ($TlAs_3S_5$), ralphcannonite ($AgZn_2TlAs_2S_6$) and ferrostalderite ($CuFe_2TlAs_2S_6$), respectively. Approved by IMA-CNMNC but not yet published are richardsollyite (IMA 2016-043, $TlPbAsS_3$), argentoliveingite (IMA 2016-029, $Ag_xPb_{40-2x}As_{48+x}S_{112}$, with $3 < x < 4$) and argentodufrénoysite (IMA 2016-046, $Ag_3Pb_{26}As_{35}S_{80}$) by Meisser *et al.* (2017) and Topa *et al.* (2016a, b), respectively.

Our studied samples come from material collected between 1816 and 2015 at the Lengenbach quarry, Binntal, Switzerland. Altogether, 232 samples were made available to us by the following persons (in chronological order): Peter Berlepsch (Switzerland), Horst Geuer (Germany), Frank Keutsch (Germany), Uwe Kolitsch (Austria), Thomas Raber (Germany), Phillippe Roth (Switzerland) and Ralph Cannon (Germany) from their private collections. As curator, Uwe Kolitsch also provided selected material from 23 samples from the mineralogical collection of the Natural History Museum-Wien.

Heptasartorite was found for the first time in a sample provided by Horst Geuer to the first author and after that in a sample from the mineral collection of NHM-Wien. No

Table 1. Reflectance data (%) for M-sartorites (in air).

| λ (nm) | Heptasartorite | | Enneasartorite | | Hendekasartorite | |
|---|---|---|---|---|---|---|
| | $R_1$ | $R_2$ | $R_1$ | $R_2$ | $R_1$ | $R_2$ |
| 400 | 38.7 | 41.9 | 39.2 | 41.6 | 39.5 | 42.5 |
| 420 | 37.7 | 41.1 | 38.3 | 40.9 | 38.7 | 41.8 |
| 440 | 36.9 | 40.5 | 37.6 | 40.4 | 38.0 | 41.3 |
| 460 | 36.3 | 40.2 | 37.0 | 40.0 | 37.5 | 40.8 |
| **470** | **36.0** | **40.0** | **36.7** | **39.7** | **37.2** | **40.6** |
| 480 | 35.7 | 39.7 | 36.4 | 39.5 | 37.1 | 40.4 |
| 500 | 35.2 | 39.0 | 35.9 | 38.9 | 36.7 | 40.0 |
| 520 | 34.5 | 38.3 | 35.2 | 38.3 | 36.2 | 39.5 |
| 540 | 33.7 | 37.5 | 34.5 | 37.6 | 35.6 | 38.9 |
| **546** | **33.5** | **37.5** | **34.0** | **37.2** | **35.3** | **38.5** |
| 560 | 33.0 | 36.7 | 33.7 | 36.8 | 35.0 | 38.1 |
| 580 | 32.2 | 35.8 | 32.9 | 35.8 | 34.3 | 37.2 |
| **589** | **31.7** | **35.3** | **32.4** | **35.4** | **33.9** | **36.8** |
| 600 | 31.4 | 34.9 | 32.0 | 34.9 | 33.4 | 36.3 |
| 620 | 30.6 | 34.0 | 31.2 | 34.0 | 32.6 | 35.3 |
| 640 | 29.9 | 33.2 | 30.5 | 33.1 | 31.8 | 34.4 |
| **650** | **29.6** | **32.8** | **30.2** | **32.8** | **31.5** | **34.0** |
| 660 | 29.3 | 32.6 | 29.9 | 32.4 | 31.1 | 33.6 |
| 680 | 28.9 | 32.2 | 29.4 | 31.9 | 30.5 | 32.9 |
| 700 | 28.7 | 31.8 | 29.2 | 31.6 | 30.1 | 32.4 |

The reference wavelengths required by the Commission on Ore Mineralogy (COM) are given in bold.

Fig. 1. Optical image of an enneasartorite–baumhauerite aggregate (sample HG039). Field of view is 2 mm. (Sample courtesy of Horst Geuer; photo by Matthias Reinhardt.)

other sample of heptasartorite was found so far. Enneasartorite and hendekasartorite were identified in a number of samples, being common in the investigated samples (Fig. 1). The exact time of acquisition and location in the quarry are unknown for all samples containing the three new minerals. We believe that the place and time is that of a Tl-rich zone at Lengenbach quarry in the mid-eighties of the past century.

## 3. Physical and optical properties

There are no significant differences between physical properties of hepta-, ennea-, and hendekasartorite. All three are opaque, have a metallic lustre, a lead-grey colour and dark brown streak. Mohs hardness equal to 3–3½ was derived from the micro-indentation test for all of them. The micro-indentation hardness $VHN_{25}$ tests yielded: mean value of 202 kg mm$^{-2}$ (range 194–211) for heptasartorite, mean value of 206 kg mm$^{-2}$ (range 199–213) for enneasartorite and mean value of 214 kg mm$^{-2}$ (range 208–221) for hendekasartorite. All minerals are brittle, with good cleavage {1 0 0}. No parting was observed and fracture is brittle-conchoidal. The density of all three minerals could not be measured because of paucity of available material and of intergrowths of mineral species; $D_{(calc.)}$ is equal to 4.9 g cm$^{-3}$ for heptasartorite, to 5.1 g cm$^{-3}$ for enneasartorite and to 5.18 g cm$^{-3}$ for hendekasartorite using the simplified formulae given below.

This makes it obvious that the members of the sartorite anion-omission series cannot be distinguished by physical properties alone. Ideal crystals would display different vicinal faces, but the quality of real crystals does not match the requirements.

There are no conspicuous differences between qualitative optical properties of hepta-, ennea- and hendekasartorite in reflected light in polished sections. They are greyish-white, internal reflections are rare but deep red for all three phases where present. Bireflectance and pleochroism are weak, anisotropy is moderate to weak, in brown-violet and deep green tones. Slight differences in reflectance values are to be expected because of changing Pb/(Tl+As) ratios in them. Measurements were obtained with a WTiC standard in air and are shown in Table 1 and Fig. 2.

Both the maximum and minimum reflectance values increase slightly from heptasartorite to hendekasartorite, as expected, although the observed increase is slight and

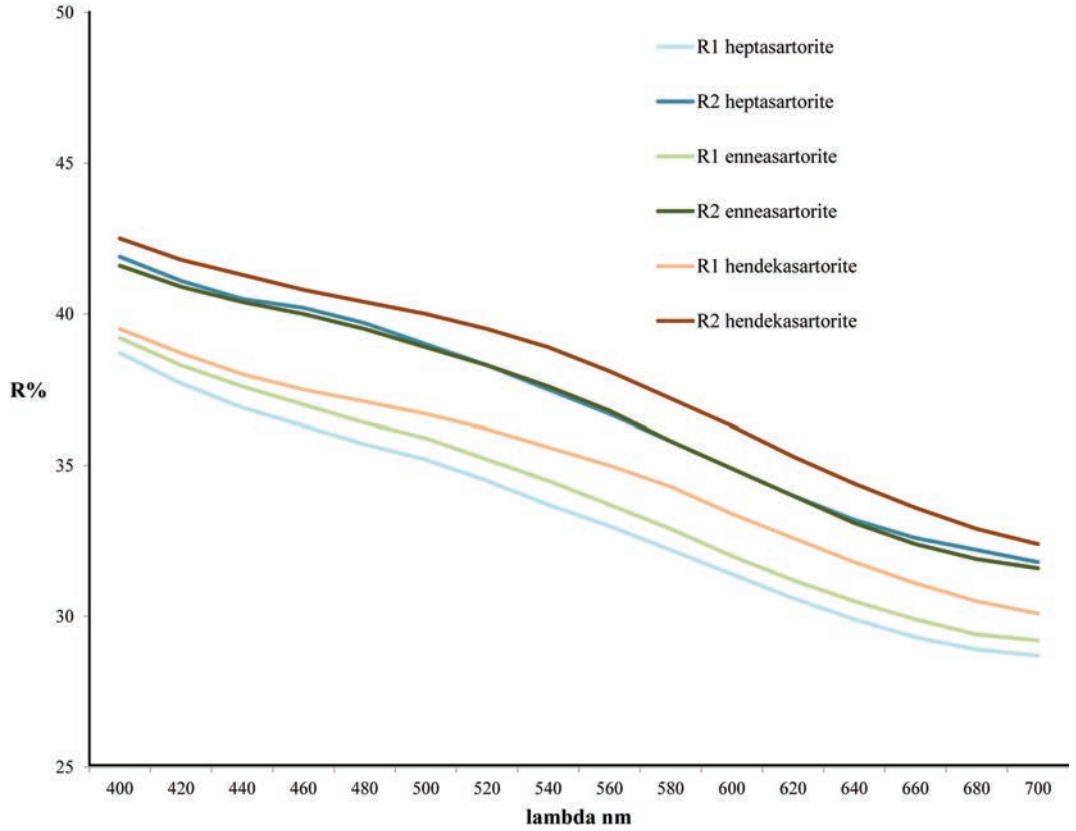


Fig. 2. Reflectance data (%) for heptasartorite, enneasartorite and hendekasartorite.

Table 2. Composition of M-sartorites (wt%).

| No. | Mineral | | *n*(gr)* | Tl | Pb | As | Sb | S | Total | *ch*** | $N_{calc}$*** | $Tl_{subst}$*** |
|---|---|---|---|---|---|---|---|---|---|---|---|---|
| 1 | Heptasartorite | Mean | 15(3) | 10.98 | 32.83 | 29.72 | 1.18 | 25.44 | 100.15 | 0.25 | 3.51 | 63 |
| | | *sd* | | *0.23* | *0.37* | *0.21* | *0.10* | *0.17* | *0.22* | | | |
| 2 | Enneasartorite | Mean | 12(3) | 7.44 | 37.17 | 28.99 | 1.09 | 25.42 | 100.12 | −0.12 | 3.42 | 46 |
| | | *sd* | | *0.11* | *0.38* | *0.25* | *0.31* | *0.18* | *0.26* | | | |
| 3 | Hendekasartorite | Mean | 22(5) | 2.80 | 44.63 | 27.10 | 0.90 | 24.83 | 100.26 | 0.29 | 3.38 | 18 |
| | | *sd* | | *0.15* | *0.20* | *0.14* | *0.06* | *0.13* | *0.31* | | | |

* *n* – number of analyses; (gr) – number of grains; ** *ch* – charge balance (Σcations−Σanions) based on at%; *** $N_{calc}$ and $Tl_{subst}$ as described in text. *sd* – standard deviation. Empirical formulae, on the basis of 192, 248 and 304 *apfu*, respectively (from single-crystal study).
1. $Tl_{7.30}Pb_{21.55}(As_{53.94}Sb_{1.31})_{\Sigma 55.25}S_{107.90}$ ΣMe = 84.10.
2. $Tl_{6.42}Pb_{31.68}(As_{68.31}Sb_{1.59})_{\Sigma 69.90}S_{140.00}$ ΣMe = 108.00.
3. $Tl_{3.03}Pb_{47.71}(As_{80.10}Sb_{1.65})_{\Sigma 81.74}S_{171.52}$ ΣMe = 132.48.

cannot be used as diagnostic tool (variability with grain orientation will have greater influence than this difference).

## 4. Chemical composition

Chemical analyses of heptasartorite, enneasartorite and hendekasartorite were carried out using a JEOL JXA 8530F field-emission-gun electron microprobe in the Central Laboratory at the Natural History Museum Vienna employing JEOL and PROBE software (wavelength-dispersive mode, 25 kV, 20 nA, 2-μm beam diameter, 10-s count time on peak and 5 s on background positions). Raw X-ray intensities were corrected for matrix effects with a ZAF procedure. Other elements (Hg, Cu, Fe and Ag) were sought for but not detected. The following emission lines and standards were used: As-*L*α Tl-*L*α and S-*K*α (lorándite $TlAsS_2$), Pb-*M*α (galena PbS) and Sb-*L*α (stibnite $Sb_2S_3$). The mean chemical compositions (and number of point analyses, NA) for all three new minerals used for structural studies are presented in Table 2 and plotted in the (As + Sb)–Tl–Pb ternary diagram (Fig. 3). Chemical analyses of all minerals show that Tl is a major element, whereas Sb is minor and Ag entirely missing. The

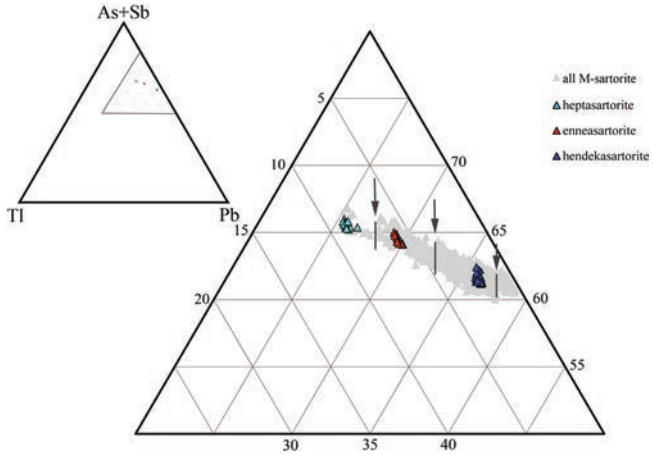


Fig. 3. Analytical data points of the structurally characterized hepta-, ennea- and hendekasartorite from Lengenbach in a portion of Pb–As(+ minor Sb)–Tl diagram (at% of cations). Grey background: data points for all M-sartorite samples from Lengenbach analyzed during this study; probable boundaries between the composition fields of the three minerals are indicated.

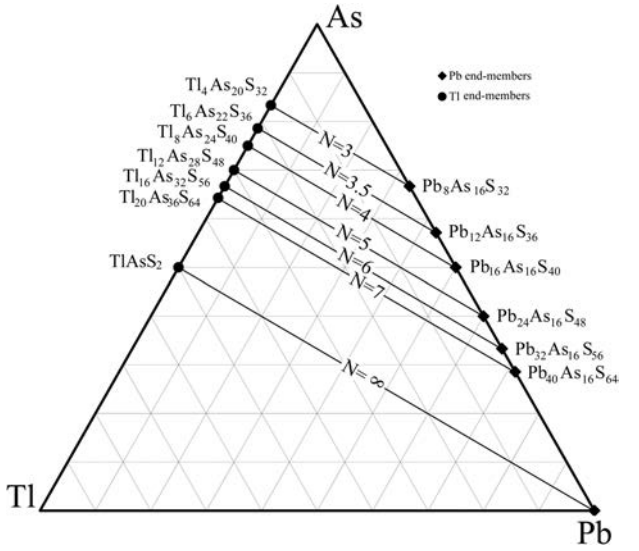


Fig. 4. Trend of $N$ values in the sartorite homologous series for the case of $Tl + As \leftrightarrow 2Pb$ substitution (mol% of sulfide components). $N = 3.67$ not plotted, $N$ larger than 4 has not yet been found.

boundaries between the compositional fields of the new minerals are set on the basis of their associations and a clear definition of these boundaries is ongoing.

The chemistry of the phases belonging to the sartorite family can be interpreted from a large number of analyses on the basis of the calculated sartorite homologue number – $N_{chem}$, defined by Makovicky (1985, 1997) and improved by Makovicky & Topa (2015). The expected trend of $N$ values for the case of the $Tl + As \leftrightarrow 2Pb$ substitution is shown in Fig. 4. The theoretical value of $N_{chem}$ for the sartorite family is 3. As shown in Table 2, experimental values of $N_{chem}$ range from 3.51 to 3.38 with decreasing Tl content and deviate substantially from the ideal $N$ value. These phenomena need explanation. To this aim, correct empirical and simplified formulae are needed, both deriving from the structural formula as obtained from the single-crystal studies and structure refinements. We found for heptasartorite 192 atoms per formula unit (*apfu*), 84Me + 108S; for enneasartorite 248 *apfu*, 108Me + 140 S; for heptasartorite 304 *apfu*, 132Me + 172S and use it for appropriate empirical formula calculations (Table 2).

The structures of hepta-, ennea-, and hendekasartorite have four missing S atoms per super-period (*i.e.* = per 7-tuple to 11-tuple of the 4.2 Å period). Cation compensation of the charge imbalance caused by anion vacancies *differs from the usual* $Tl + As \leftrightarrow 2Pb$ substitution typical for the sartorite homologous series. Analysis of data indicates a combination and competition of two substitution schemes:

(a) The *Tl-substitution model of vacancy-related cation compensation*, in which $2Tl^{+}$ substitutes for $2Pb^{2+}$, resulting in one S vacancy per superperiod. The resulting formula is $Pb_{M-2}Tl_2As_{2M}S_{4M-1}$ ($Z = 4$), with ideally 2Tl per superperiod when we exclude the possible additional $Tl + As \leftrightarrow 2Pb$ exchange. This gives a composition equal to $Pb_5Tl_2As_{14}S_{27}$ for heptasartorite, $Pb_7Tl_2As_{18}S_{35}$ for enneasartorite, and $Pb_9Tl_2As_{22}S_{43}$ for hendekasartorite ($Z = 4$ for all). These formulae give the highest thallium cation-percentages in the Pb–As–Tl ternary plot (Fig. 5).

(b) The *Tl-free substitution model* combines the S vacancy with a *lead-for-arsenic substitution*: 2As atoms per superperiod will be exchanged by 2Pb atoms in order to compensate for 1 sulfur vacancy per superperiod. In the consequence, the 'ideal' formula $Pb_MAs_{2M}S_{4M}$ will be changed into $Pb_{M+2}As_{2M-2}S_{4M-1}$, *i.e.*, $Pb_9As_{12}S_{27}$ for heptasartorite, $Pb_{11}As_{16}S_{35}$ for ennea-sartorite and $Pb_{13}As_{20}S_{43}$ for hendekasartorite ($Z = 4$ for all); again see Fig. 5.

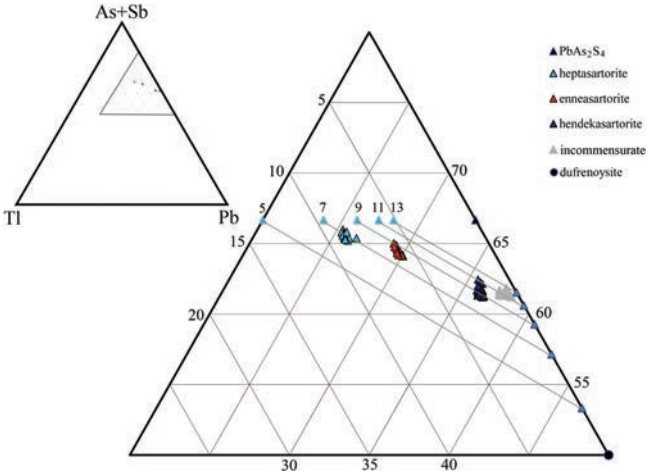


Fig. 5. Analytical data points of the structurally characterized hepta-, ennea- and hendekasartorite plotted on the background of composition lines that connect the end-points with theoretical $Tl \leftrightarrow Pb$ (left) and $Pb \leftrightarrow As$ (right margin) charge compensations for sulfur vacancies. Position of symbols on their lines indicates the proportions of the two compensation mechanisms active in each phase. Grey symbols on the right are from incommensurate phases currently under description.

The true substitution is a combination of these two competing mechanisms (considered here on a pure stoichiometric basis, without speculation on the sites involved). Good analyses lie on their proper superperiod 'M' lines, and the Tl ↔ Pb mechanism of compensation predominates for M = 7 and 9, whereas the Pb ↔ As mechanism predominates for M = 11.

As long as the Tl contents do not exceed the value of the complete vacancy compensation by Tl incorporation, we assume that all Tl present is used for the compensation and not for the simple Tl + As ↔ 2Pb exchange. For all superperiod values, the Tl value *pfu* based on 4M–1S atoms is 2. Thus, the Tl value *pfu* in the empirical formula with 4M–1S atoms (and the corresponding number of cations), divided by 2 and multiplied by 100, gives the percentage of the Tl-based vacancy compensation; the rest to 100 is the Pb ↔ As valence compensation. These principles are used below.

The empirical formula for heptasartorite (based on 192 *apfu*, 84Me + 108S) is $Tl_{7.30}Pb_{21.55}(As_{53.94}Sb_{1.31})_{\Sigma 55.25}S_{107.90}$ (ΣMe = 84.1). The crystal-structure formula is $(Tl_{<8}Pb_{>20.8})_{\Sigma 28.8}As_{55.2}S_{108}$ (ΣMe = 84). The simplified formula, $Tl_7Pb_{22}(As_{54}Sb)_{\Sigma 55}S_{108}$ is derived from the 7-fold superstructure of 'ideal sartorite' (*i.e.*, $7 \times Pb_4As_8S_{16} = Pb_{28}As_{56}S_{112}$), by a combination of sulfur omission with appropriate changes in cation ratios. Ideally, omission of 4S *pfu* entails replacement of 8Pb atoms of the 'ideal' formula by 8Tl giving $Tl_8Pb_{20}As_{56}S_{108}$. In order to satisfy some local structural constraints, this substitution competes in the real structure with a substitution of a part of As by Pb as means of vacancy charge compensation. Calculations show that vacancy charge compensation proceeds by the Tl-involving mechanism for about 87.5% and by the Pb-substitution mechanism for about 22.5%.

The empirical formula for enneasartorite (based on 248 *apfu*, 108Me + 140S) is: $Tl_{6.42}Pb_{31.68}(As_{68.31}Sb_{1.59})_{\Sigma 69.9}S_{140.0}$ (ΣMe = 107.99). The crystal-structure formula is less accurate, $(Tl_{<4}Pb_{>36.4})_{\Sigma 40.4}As_{67.6}S_{140}$ (ΣMe = 108). The simplified formula $Tl_6Pb_{32}As_{70}S_{140}$ is derived from the 9-fold superstructure of 'ideal sartorite' (*i.e.*, $9 \times Pb_4As_8S_{16} = Pb_{36}As_{72}S_{144}$), by a combination of sulfur omission with appropriate changes in cation ratios. Ideally, omission of 4S entails replacement of 8Pb atoms of the above 'ideal' formula by 8Tl and should yield $Tl_8Pb_{28}As_{72}S_{140}$. However, the Pb ↔ As substitution covers a part of compensation process; it consumes 1.6As, cancelling a need for 1.6Tl, giving $Tl_{6.4}Pb_{31.2}As_{70.4}S_{140}$, as a result, only in minor disagreement with the empirical formula given above. Thus, the Tl ↔ Pb substitution covers about 80.3% of the charge compensation.

The empirical formula for hendekasartorite (based on 304 *apfu*, 132Me + 172S) is $Tl_{3.03}Pb_{47.71}(As_{80.1}Sb_{1.65})_{\Sigma 81.74}S_{171.52}$ (ΣMe = 132.48). The crystal-structure formula is $(Pb,Tl)_{\Sigma 50.28}As_{81.72}S_{172}$ (ΣMe = 132). The simplified formula, $Tl_2Pb_{48}As_{82}S_{172}$, is derived from the 11-fold superstructure of 'ideal sartorite' (*i.e.*, $11 \times Pb_4As_8S_{16} = Pb_{44}As_{88}S_{176}$), by a combination of sulfur omission with appropriate changes in cation ratios. As it was the case in the other 'M-sartorite' species, two compensation mechanisms for the loss of sulfur (4S *apfu* of $Me_{132}S_{172}$) operate also in hendekasartorite: (1) Addition of Pb *at the expense of* As, yielding $Pb_{52}As_{80}S_{172}$; this 'end-member' covers 62.5 mol% of the observed cation charge compensation. (2) Replacement of Pb by Tl, with $Tl_8Pb_{36}As_{88}S_{172}$ as the 'end-member'; this substitution covers 37.5 mol% of the observed cation charge compensation. The combination of 'end-members' 2 and 1 in the relevant atomic proportion reads as follows: $Pb_{32.5}As_{50}S_{107.5} + Tl_3Pb_{13.5}As_{33}S_{64.5} = Tl_3Pb_{46}As_{83}S_{172}$, close to the above empirical formula.

## 5. Principal features of the crystal structures

In spite of the common structural rules, it is the unique structural features of individual members of this omission series that define them as independent species with distinct mineral names. The differences are not just the isovalent or heterovalent atom substitutions or cation ratios in solid solutions, but *they are based on introduction of new and distinct structure modules.*

All three minerals are monoclinic and crystallize in the space group $P2_1/c$ (SG#14). The unit-cell parameters of heptasartorite are $a = 29.269(2)$, $b = 7.8768(5)$, $c = 20.128(2)$ Å, $\beta = 102.065(2)°$ and unit-cell volume $V = 4537.8$ Å$^3$. Enneasartorite has $a = 37.612(6)$, $b = 7.8777(12)$, $c = 20.071(3)$ Å, $\beta = 101.930(2)°$ and $V = 5818.6(15)$ Å$^3$, whereas hendekasartorite has $a = 31.806(5)$, $b = 7.889(12)$, $c = 28.556(4)$ Å, and $\beta = 99.034(2)°$ with $V = 7076.4(15)$ Å$^3$. For the first two structures, all parameters are almost identical, with exception of the $a$ parameter which exhibits incremental growth by addition of a new module in the enneasartorite. While the $b$ direction in hendekasartorite has the same orientation as in the other 'M-sartorite' species, the $a$ and $c$ axes are oriented diagonally to those in hepta- and enneasartorite, escaping a simple comparison. Crystal structures were determined from newly collected single-crystal X-ray data, processed, and the structures were refined to the $R_1$ values of 0.052, 0.066 and 0.085, respectively.

The structures of all three minerals are typical for the $N = 3$ member of the sartorite homologous series, with the three-polyhedron-wide double ribbons which include trigonal prismatic Pb positions on the margins and As-rich portions more concentrated in the ribbon interior. Strong bonds to sulfur, especially those of As, are mostly oriented into the volume of a double-ribbon, whereas the lone-electron pairs of As point into the inter-ribbon space. A main feature of all three structures is the presence of short diagonal crankshaft chains of (especially) short As–S bonds. These chains are stacked along the 4.2 Å $a$ direction, giving the M × 4.2 Å superstructures of the idealized 'basic sartorite motif'. As refined, M = 7 and M = 11 are so far the shortest and the longest fully refined modulated direction among the 'M-sartorite structures'.

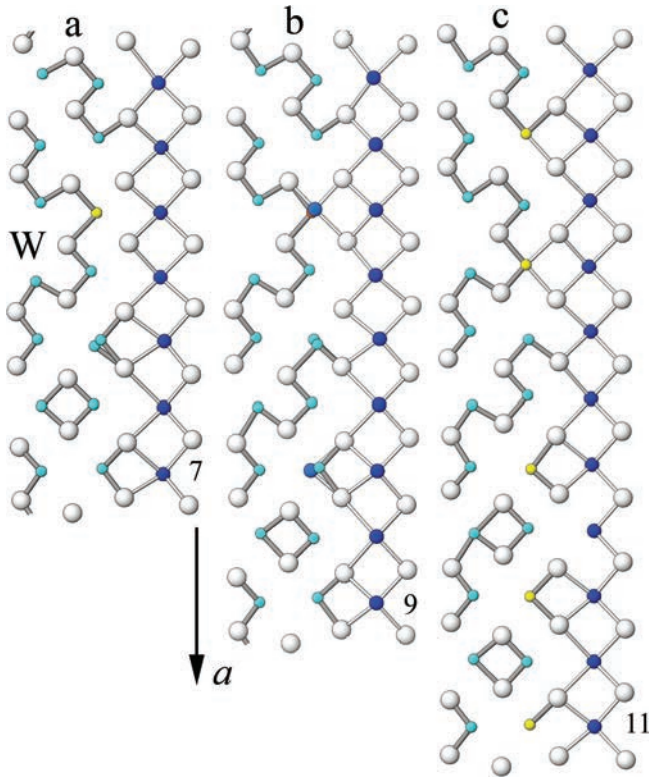


Fig. 6. Surface configurations of double-ribbons that form the SnS-like portions of the (a) hepta-, (b) ennea-, and (c) hendekasartorite structures. Atom colouring: white, sulfur; dark blue, Pb(Tl); turquoise, As; yellow, mixed cation sites. The short As–S bonds are accentuated in grey.

Detailed descriptions of these complicated structures will be given in a separate paper, but their principal and defining modular features can be described as follows. We base our description on configurations in one wall of the double-ribbon, because the motif repeats on all such surfaces. The pivotal element among these configurations in heptasartorite and other M-sartorites is a 'W-like configuration' of two amalgamated crankshaft portions with the in-plane formula $As_5Me_1S_7$ (Fig. 6). In this configuration, the Me position has been modelled as a mixed As–Pb site. The other ubiquitous configuration is a tightly bonded $As_2S_2$ group occurring approximately half-way between the adjacent periodic W-shaped configurations. Of course, both groups have additional strongly bonded S atoms which are situated on the other surface of the double-ribbon. In heptasartorite these two groups are separated by a short crankshaft chain $As_4S_5$ in one interval but they are immediately adjacent in the alternating interval of the double-ribbon face (Fig. 6a).

In enneasartorite the same pivotal groups occur but the $As_4S_5$ chain is opposed by a similar, $As_4S_{5(+1)}$ group with a split terminal As position. This adds two 4.2 Å periods to the superperiod, bringing multiplicity to ninefold and creating a near-symmetrical disposition of modules around the W-shaped configuration and/or around the $As_2S_2$ group (Fig. 6b). Expansion from enneasartorite to hendekasartorite proceeds by incorporation of one more $As_4S_5$ crankshaft chain on one side of the W-shaped chain configuration (Fig. 6c). The asymmetric one-inserted-chain *versus* two-inserted-chains arrangement created in this way is so far the upper limit for ordered structures of 'M-sartorites'. In all these structures, the $As_2S_2$ group is accompanied by two $AsS_2$ groups in the same ribbon surface. Importantly, the *missing sulfur* is the site chelated/clammed by the W-shaped configuration, especially by the lone-electron pairs of two As atoms facing the vacancy.

The described schemes, developed on the opposing faces of double ribbons, are displaced against one another, depending on the multiplicity of the superstructure. Details of this and of the stacking of consecutive double-layers will be described in the structural paper.

On a pure geometrical basis, transition from one M to another means addition of a block 8.4 Å large, with the same fragments of crankshaft chains; its composition and orientation are the same for both steps (Fig. 6).

## 6. Powder diffraction data

Experimental powder patterns could not be obtained from the 'M-sartorites' because of scarcity of the material and frequent intergrowths of at least two species of the sartorite homologues. The theoretical patterns (Tables 3a–c) were calculated with the PowderCell 2.3 software (Kraus & Nolze, 1999) in Debye–Scherrer configuration employing Cu$K\alpha$ radiation ($\lambda = 1.540598$ Å), a fixed slit, and no anomalous dispersion, for $I_{rel} > 2$. Cell parameters, space group, atom positions, site occupancy factors and isotropic displacement factors from the crystal-structure determination were used.

The strong reflections are common to all patterns, although with different Miller indices. Many weaker reflections do the same (at least in two patterns); species-specific reflections are rare and weak. Interestingly, there are a number of *hkl* reflection pairs of the type *hkl versus* $-h...k...(l+n)$, with $n$ between 2 and 4, that have nearly the same $d$ values and similar intensities. This is a result of lattice geometry and structure configurations of hepta- and enneasartorite. An example for the above complex relationships is the reflections of heptasartorite with $d$ equal to 2.753 Å ($-7\,2\,3$) and 2.752 Å (7 2 1) and those of enneasartorite with $d$ equal to 2.752 Å (9 2 1) and 2.751 ($-9\,2\,3$). The different lattice of hendekasartorite precludes such a way of indexing [*cf.* 2.753 Å ($-8\,2\,3$) and 2.751 Å ($-4\,2\,7$)].

## 7. Association with other sartorite homologues

The sulfosalt mineralization is widely disseminated in the dolomite gangue, with different mineralization periods situated in different portions of the deposit. As the sampling was mostly performed by mineral collectors, the textural relationships between M-sartorites and other minerals, and those of one M-sartorite type to another, are

Table 3a. Calculated X-ray powder diffraction data for heptasartorite.*

| $I_{rel}$ | $d$/Å | $h$ | $k$ | $l$ | $I_{rel}$ | $d$/Å | $h$ | $k$ | $l$ | $I_{rel}$ | $d$/Å | $h$ | $k$ | $l$ |
|---|---|---|---|---|---|---|---|---|---|---|---|---|---|---|
| 4 | 9.97 | −1 | 0 | 2 | 3 | 2.799 | 6 | 2 | 2 | 5 | 1.931 | 0 | 4 | 2 |
| **72** | **9.84** | **0** | **0** | **2** | 19 | 2.784 | 0 | 2 | 5 | 2 | 1.930 | 14 | 1 | 1 |
| 18 | 7.31 | 0 | 1 | 1 | **73** | **2.753** | **−7** | **2** | **3** | 9 | 1.919 | 0 | 3 | 7 |
| 3 | 6.90 | 2 | 1 | 0 | **73** | **2.752** | **7** | **2** | **1** | 9 | 1.912 | 0 | 2 | 9 |
| 36 | 6.15 | 0 | 1 | 2 | 4 | 2.739 | −10 | 1 | 1 | 2 | 1.900 | 10 | 3 | 1 |
| 5 | 6.07 | 3 | 1 | 0 | 3 | 2.738 | 3 | 1 | 6 | 2 | 1.883 | −7 | 1 | 10 |
| 3 | 5.86 | 1 | 1 | 2 | 2 | 2.719 | 8 | 1 | 3 | 4 | 1.870 | −14 | 1 | 6 |
| 5 | 5.04 | 0 | 1 | 3 | 4 | 2.686 | −1 | 1 | 7 | 6 | 1.868 | 14 | 1 | 2 |
| 3 | 4.93 | 4 | 1 | 1 | 27 | 2.648 | 0 | 1 | 7 | 10 | 1.868 | −7 | 2 | 9 |
| 4 | 4.92 | 0 | 0 | 4 | 20 | 2.628 | −7 | 2 | 4 | 8 | 1.866 | 7 | 2 | 7 |
| 3 | 4.80 | −3 | 0 | 4 | 27 | 2.626 | 7 | 2 | 2 | 3 | 1.847 | −14 | 2 | 2 |
| 2 | 4.47 | −4 | 1 | 3 | 3 | 2.610 | 6 | 1 | 5 | 4 | 1.841 | −7 | 3 | 7 |
| 2 | 4.39 | 4 | 1 | 2 | 4 | 2.603 | 0 | 3 | 1 | 5 | 1.840 | 7 | 3 | 5 |
| 33 | 4.17 | 0 | 1 | 4 | 12 | 2.537 | 0 | 3 | 2 | 7 | 1.839 | −14 | 2 | 3 |
| 19 | 4.09 | −7 | 0 | 2 | 2 | 2.480 | −11 | 1 | 3 | 5 | 1.838 | −14 | 2 | 1 |
| 40 | 4.09 | 7 | 0 | 0 | 3 | 2.460 | 0 | 0 | 8 | 4 | 1.828 | 0 | 4 | 4 |
| 4 | 4.04 | 3 | 0 | 4 | 5 | 2.454 | −7 | 1 | 7 | 4 | 1.815 | −14 | 2 | 4 |
| 3 | 4.03 | 1 | 1 | 4 | 7 | 2.451 | 7 | 1 | 5 | 3 | 1.800 | 6 | 3 | 6 |
| 15 | 3.94 | 0 | 2 | 0 | 2 | 2.413 | 1 | 3 | 3 | 10 | 1.799 | −14 | 1 | 7 |
| 3 | 3.90 | 1 | 2 | 0 | 6 | 2.348 | 0 | 1 | 8 | 10 | 1.797 | 14 | 1 | 3 |
| **59** | **3.86** | **0** | **2** | **1** | 23 | 2.335 | −7 | 0 | 8 | 2 | 1.789 | 10 | 3 | 3 |
| 3 | 3.66 | −1 | 2 | 2 | 25 | 2.332 | 7 | 0 | 6 | 11 | 1.782 | −7 | 4 | 1 |
| 28 | 3.66 | 0 | 2 | 2 | 26 | 2.316 | 0 | 3 | 4 | 2 | 1.778 | −1 | 2 | 10 |
| 4 | 3.58 | −1 | 1 | 5 | 9 | 2.288 | 0 | 2 | 7 | 3 | 1.777 | 14 | 2 | 1 |
| 17 | 3.53 | −7 | 0 | 4 | 12 | 2.238 | −7 | 1 | 8 | 7 | 1.774 | −7 | 4 | 2 |
| 14 | 3.52 | 7 | 0 | 2 | 11 | 2.236 | 7 | 1 | 6 | 5 | 1.774 | 7 | 4 | 0 |
| **100** | **3.52** | **0** | **1** | **5** | 6 | 2.210 | −7 | 3 | 2 | 3 | 1.764 | −14 | 0 | 8 |
| 4 | 3.46 | −6 | 1 | 4 | 5 | 2.209 | 7 | 3 | 0 | 3 | 1.757 | 10 | 2 | 6 |
| 46 | 3.46 | −7 | 1 | 3 | 2 | 2.197 | −1 | 3 | 5 | 10 | 1.745 | 0 | 1 | 11 |
| **51** | **3.46** | **7** | **1** | **1** | 2 | 2.169 | −7 | 3 | 3 | 3 | 1.745 | −7 | 3 | 8 |
| 21 | 3.38 | 0 | 2 | 3 | 7 | 2.106 | −7 | 3 | 4 | 2 | 1.744 | 7 | 3 | 6 |
| 5 | 3.36 | 4 | 1 | 4 | 7 | 2.105 | 7 | 3 | 2 | 4 | 1.740 | −7 | 2 | 10 |
| 3 | 3.32 | −3 | 0 | 6 | 41 | 2.091 | −14 | 0 | 2 | 3 | 1.738 | 7 | 2 | 8 |
| 16 | 3.28 | 0 | 0 | 6 | 14 | 2.050 | 0 | 3 | 6 | 2 | 1.738 | −7 | 1 | 11 |
| 27 | 3.22 | −7 | 1 | 4 | 2 | 2.047 | 7 | 1 | 7 | 2 | 1.730 | −14 | 2 | 6 |
| 25 | 3.22 | 7 | 1 | 2 | 4 | 2.046 | −14 | 0 | 4 | 3 | 1.721 | −14 | 1 | 8 |
| 23 | 3.07 | 0 | 2 | 4 | 3 | 2.044 | 14 | 0 | 0 | 3 | 1.680 | 0 | 3 | 9 |
| 4 | 3.06 | −3 | 1 | 6 | 3 | 1.980 | −14 | 1 | 4 | 3 | 1.675 | −7 | 4 | 5 |
| 2 | 3.04 | 6 | 2 | 0 | 5 | 1.968 | 0 | 0 | 10 | 5 | 1.642 | −14 | 1 | 9 |
| 25 | 3.03 | 0 | 1 | 6 | 6 | 1.959 | 0 | 4 | 1 | 3 | 1.640 | 14 | 1 | 5 |
| **75** | **2.955** | **−7** | **1** | **5** | 7 | 1.939 | −7 | 0 | 10 | 2 | 1.622 | 7 | 2 | 9 |
| **58** | **2.952** | **7** | **1** | **3** | 5 | 1.937 | 7 | 0 | 8 | 2 | 1.614 | −14 | 3 | 4 |
| 2 | 2.931 | 8 | 1 | 2 | 12 | 1.937 | −7 | 3 | 6 | 3 | 1.613 | 14 | 3 | 0 |
| 37 | 2.867 | −7 | 2 | 1 | 12 | 1.935 | 7 | 3 | 4 | 6 | 1.553 | −14 | 3 | 6 |

* The theoretical pattern was calculated with *PowderCell* 2.3 software (Kraus & Nolze, 1999) in Debye–Scherrer configuration employing Cu$K\alpha$ radiation ($\lambda = 1.540598$ Å), a fixed slit, and no anomalous dispersion, for $I_{rel} > 2$. Cell parameters, space group, atom positions, site occupancy factors and isotropic displacement factors from the crystal structure determination were used.
The strongest lines are given in bold.

Table 3b. Calculated X-ray powder diffraction data for enneasartorite (see Table 3a, footnote).

| $I_{rel}$ | $d$/Å | $h$ | $k$ | $l$ | $I_{rel}$ | $d$/Å | $h$ | $k$ | $l$ | $I_{rel}$ | $d$/Å | $h$ | $k$ | $l$ |
|---|---|---|---|---|---|---|---|---|---|---|---|---|---|---|
| 3 | 10.02 | −1 | 0 | 2 | **76** | **2.949** | **−9** | 1 | 5 | 6 | 1.933 | −9 | 0 | 10 |
| **67** | **9.82** | **0** | **0** | **2** | 38 | 2.866 | −9 | 2 | 1 | 5 | 1.931 | 0 | 4 | 2 |
| 18 | 7.31 | 0 | 1 | 1 | 19 | 2.781 | 0 | 2 | 5 | 9 | 1.917 | 0 | 3 | 7 |
| 2 | 6.63 | 3 | 1 | 0 | 3 | 2.769 | 10 | 1 | 3 | 7 | 1.909 | 0 | 2 | 9 |
| 32 | 6.14 | 0 | 1 | 2 | 2 | 2.760 | 8 | 2 | 2 | 2 | 1.890 | 13 | 3 | 1 |
| 2 | 5.98 | 4 | 1 | 0 | **71** | **2.752** | **9** | 2 | 1 | 5 | 1.869 | 18 | 1 | 2 |
| 3 | 5.94 | 1 | 1 | 2 | **73** | **2.751** | **−9** | 2 | 3 | 4 | 1.867 | −18 | 1 | 6 |
| 7 | 5.03 | 0 | 1 | 3 | 2 | 2.743 | 1 | 2 | 5 | 8 | 1.865 | 9 | 2 | 7 |
| 2 | 5.00 | 5 | 1 | 1 | 3 | 2.722 | 4 | 1 | 6 | 10 | 1.863 | −9 | 2 | 9 |

Table 3b. (continued).

| $I_{rel}$ | $d$/Å | $h$ | $k$ | $l$ | $I_{rel}$ | $d$/Å | $h$ | $k$ | $l$ | $I_{rel}$ | $d$/Å | $h$ | $k$ | $l$ |
|---|---|---|---|---|---|---|---|---|---|---|---|---|---|---|
| 4 | 4.91 | 0 | 0 | 4 | 3 | 2.711 | −13 | 1 | 1 | 3 | 1.846 | −18 | 2 | 2 |
| 4 | 4.76 | −4 | 0 | 4 | 4 | 2.673 | −1 | 1 | 7 | 4 | 1.840 | 9 | 3 | 5 |
| 2 | 4.44 | 5 | 1 | 2 | 26 | 2.643 | 0 | 1 | 7 | 3 | 1.838 | −9 | 3 | 7 |
| 32 | 4.17 | 0 | 1 | 4 | 28 | 2.627 | 9 | 2 | 2 | 5 | 1.838 | −18 | 2 | 1 |
| 36 | 4.09 | 9 | 0 | 0 | 24 | 2.625 | −9 | 2 | 4 | 7 | 1.838 | −18 | 2 | 3 |
| 23 | 4.09 | −9 | 0 | 2 | 3 | 2.603 | 0 | 3 | 1 | 3 | 1.828 | 0 | 4 | 4 |
| 2 | 4.06 | 1 | 1 | 4 | 4 | 2.573 | 8 | 1 | 5 | 4 | 1.814 | −18 | 2 | 4 |
| 2 | 4.00 | 4 | 0 | 4 | 3 | 2.538 | −14 | 1 | 2 | 9 | 1.797 | 18 | 1 | 3 |
| 15 | 3.94 | 0 | 2 | 0 | 13 | 2.537 | 0 | 3 | 2 | 10 | 1.795 | −18 | 1 | 7 |
| 3 | 3.92 | 1 | 2 | 0 | 3 | 2.455 | 0 | 0 | 8 | 3 | 1.787 | 8 | 3 | 6 |
| **63** | **3.86** | **0** | **2** | **1** | 6 | 2.451 | 9 | 1 | 5 | 12 | 1.782 | −9 | 4 | 1 |
| 34 | 3.66 | 0 | 2 | 2 | 6 | 2.447 | −9 | 1 | 7 | 3 | 1.780 | 13 | 3 | 3 |
| 2 | 3.63 | 9 | 1 | 0 | 6 | 2.344 | 0 | 1 | 8 | 4 | 1.774 | 9 | 4 | 0 |
| 2 | 3.63 | −9 | 1 | 2 | 24 | 2.331 | 9 | 0 | 6 | 7 | 1.774 | −9 | 4 | 2 |
| 5 | 3.56 | −1 | 1 | 5 | 25 | 2.328 | −9 | 0 | 8 | 3 | 1.760 | −18 | 0 | 8 |
| 14 | 3.52 | 9 | 0 | 2 | 26 | 2.315 | 0 | 3 | 4 | 3 | 1.742 | −9 | 3 | 8 |
| 17 | 3.52 | −9 | 0 | 4 | 10 | 2.285 | 0 | 2 | 7 | 10 | 1.741 | 0 | 1 | 11 |
| **100** | **3.51** | **0** | **1** | **5** | 10 | 2.235 | 9 | 1 | 6 | 3 | 1.737 | 9 | 2 | 8 |
| **51** | **3.46** | **9** | **1** | **1** | 12 | 2.232 | −9 | 1 | 8 | 5 | 1.735 | −9 | 2 | 10 |
| 47 | 3.45 | −9 | 1 | 3 | 7 | 2.210 | 9 | 3 | 0 | 2 | 1.733 | −9 | 1 | 11 |
| 3 | 3.40 | −8 | 1 | 4 | 7 | 2.209 | −9 | 3 | 2 | 2 | 1.727 | −18 | 2 | 6 |
| 4 | 3.38 | 5 | 1 | 4 | 2 | 2.168 | −9 | 3 | 3 | 3 | 1.718 | −18 | 1 | 8 |
| 20 | 3.37 | 0 | 2 | 3 | 2 | 2.120 | 8 | 1 | 7 | 3 | 1.678 | 0 | 3 | 9 |
| 2 | 3.31 | −4 | 0 | 6 | 8 | 2.106 | 9 | 3 | 2 | 3 | 1.674 | −9 | 4 | 5 |
| 17 | 3.27 | 0 | 0 | 6 | 8 | 2.105 | −9 | 3 | 4 | 3 | 1.640 | 18 | 1 | 5 |
| 26 | 3.22 | 9 | 1 | 2 | 42 | 2.090 | −18 | 0 | 2 | 5 | 1.638 | −18 | 1 | 9 |
| 26 | 3.21 | −9 | 1 | 4 | 16 | 2.048 | 0 | 3 | 6 | 2 | 1.621 | 9 | 2 | 9 |
| 2 | 3.20 | 1 | 0 | 6 | 2 | 2.044 | 18 | 0 | 0 | 2 | 1.619 | −9 | 2 | 11 |
| 2 | 3.10 | 4 | 1 | 5 | 3 | 2.043 | −18 | 0 | 4 | 3 | 1.613 | 18 | 3 | 0 |
| 25 | 3.07 | 0 | 2 | 4 | 2 | 1.978 | −18 | 1 | 4 | 3 | 1.613 | −18 | 3 | 4 |
| 2 | 3.05 | −4 | 1 | 6 | 5 | 1.964 | 0 | 0 | 10 | 4 | 1.552 | 18 | 3 | 2 |
| 24 | 3.02 | 0 | 1 | 6 | 7 | 1.960 | 0 | 4 | 1 | 6 | 1.551 | −18 | 3 | 6 |
| 3 | 2.992 | 8 | 2 | 0 | 13 | 1.936 | 9 | 3 | 4 | 3 | 1.543 | 18 | 2 | 5 |
| 3 | 2.991 | 10 | 1 | 2 | 5 | 1.935 | 9 | 0 | 8 | 2 | 1.541 | −18 | 2 | 9 |
| **61** | **2.953** | **9** | **1** | **3** | 13 | 1.934 | −9 | 3 | 6 | | | | | |

Table 3c. Calculated X-ray powder diffraction data for hendekasartorite (see Table 3a, footnote).

| $I_{rel}$ | $d$/Å | $h$ | $k$ | $l$ | $I_{rel}$ | $d$/Å | $h$ | $k$ | $l$ | $I_{rel}$ | $d$/Å | $h$ | $k$ | $l$ |
|---|---|---|---|---|---|---|---|---|---|---|---|---|---|---|
| 3 | 12.17 | 1 | 0 | 2 | 24 | 2.623 | −3 | 2 | 8 | 4 | 1.864 | −8 | 1 | 14 |
| **56** | **9.76** | **2** | **0** | **2** | 3 | 2.606 | 1 | 3 | 1 | 11 | 1.860 | 14 | 2 | 3 |
| 18 | 7.31 | 1 | 1 | 1 | 3 | 2.556 | −9 | 1 | 8 | 12 | 1.857 | 2 | 2 | 13 |
| 32 | 6.14 | 2 | 1 | 2 | 14 | 2.539 | 2 | 3 | 2 | 3 | 1.846 | −12 | 2 | 10 |
| 10 | 5.02 | 3 | 1 | 3 | 5 | 2.443 | 12 | 1 | 1 | 6 | 1.838 | −13 | 2 | 9 |
| 3 | 4.88 | 4 | 0 | 4 | 4 | 2.440 | 8 | 0 | 8 | 4 | 1.838 | 12 | 3 | 1 |
| 4 | 4.55 | 1 | 0 | 6 | 5 | 2.438 | 0 | 1 | 11 | 7 | 1.838 | −11 | 2 | 11 |
| 35 | 4.15 | 4 | 1 | 4 | 7 | 2.331 | 8 | 1 | 8 | 4 | 1.836 | 0 | 3 | 11 |
| 33 | 4.09 | −7 | 0 | 4 | 28 | 2.322 | 13 | 0 | 2 | 3 | 1.829 | 4 | 4 | 4 |
| 25 | 4.08 | −5 | 0 | 6 | 28 | 2.317 | 1 | 0 | 12 | 2 | 1.815 | −14 | 2 | 8 |
| 12 | 3.94 | 0 | 2 | 0 | 29 | 2.315 | 4 | 3 | 4 | 3 | 1.813 | −10 | 2 | 12 |
| **69** | **3.87** | **1** | **2** | **1** | 14 | 2.277 | 7 | 2 | 7 | 10 | 1.795 | −17 | 1 | 5 |
| 37 | 3.66 | 2 | 2 | 2 | 12 | 2.227 | 13 | 1 | 2 | 10 | 1.792 | −7 | 1 | 15 |
| 3 | 3.63 | −7 | 1 | 4 | 13 | 2.223 | 1 | 1 | 12 | 2 | 1.786 | −13 | 3 | 3 |
| 3 | 3.63 | −5 | 1 | 6 | 9 | 2.212 | −7 | 3 | 4 | 12 | 1.784 | −6 | 4 | 5 |
| 14 | 3.52 | −9 | 0 | 2 | 9 | 2.211 | −5 | 3 | 6 | 6 | 1.776 | −7 | 4 | 4 |
| 15 | 3.51 | −3 | 0 | 8 | 2 | 2.169 | −4 | 3 | 7 | 7 | 1.776 | −5 | 4 | 6 |
| **100** | **3.50** | **5** | **1** | **5** | 8 | 2.107 | −9 | 3 | 2 | 3 | 1.756 | −6 | 0 | 16 |
| **51** | **3.46** | **−8** | **1** | **3** | 8 | 2.105 | −3 | 3 | 8 | 4 | 1.731 | 15 | 2 | 4 |
| 49 | 3.45 | −4 | 1 | 7 | 45 | 2.089 | −12 | 0 | 10 | 13 | 1.731 | 11 | 1 | 11 |
| 18 | 3.37 | 3 | 2 | 3 | 18 | 2.045 | 6 | 3 | 6 | 5 | 1.728 | 3 | 2 | 14 |
| 4 | 3.30 | 8 | 1 | 2 | 2 | 2.044 | −14 | 0 | 8 | 2 | 1.728 | −16 | 2 | 6 |

Table 3c. (continued).

| $I_{rel}$ | $d$/Å | $h$ | $k$ | $l$ | $I_{rel}$ | $d$/Å | $h$ | $k$ | $l$ | $I_{rel}$ | $d$/Å | $h$ | $k$ | $l$ |
|---|---|---|---|---|---|---|---|---|---|---|---|---|---|---|
| 21 | 3.25 | 6 | 0 | 6 | 3 | 2.042 | −10 | 0 | 12 | 3 | 1.726 | −8 | 2 | 14 |
| 30 | 3.21 | −9 | 1 | 2 | 2 | 2.001 | 13 | 2 | 2 | 2 | 1.717 | −18 | 1 | 4 |
| 30 | 3.21 | −3 | 1 | 8 | 2 | 1.998 | 1 | 2 | 12 | 3 | 1.714 | −6 | 1 | 16 |
| 31 | 3.07 | 4 | 2 | 4 | 8 | 1.962 | 1 | 4 | 1 | 2 | 1.675 | −2 | 4 | 9 |
| 25 | 3.01 | 6 | 1 | 6 | 6 | 1.952 | 10 | 0 | 10 | 3 | 1.673 | 9 | 3 | 9 |
| **66** | **2.947** | **−10** | **1** | **1** | 14 | 1.934 | 11 | 3 | 0 | 3 | 1.637 | −19 | 1 | 3 |
| **76** | **2.941** | **−2** | **1** | **9** | 7 | 1.933 | 2 | 4 | 2 | 4 | 1.634 | −5 | 1 | 17 |
| 40 | 2.868 | −6 | 2 | 5 | 15 | 1.932 | −1 | 3 | 10 | 2 | 1.618 | 11 | 2 | 11 |
| 22 | 2.775 | 5 | 2 | 5 | 6 | 1.927 | 15 | 0 | 4 | 3 | 1.615 | 16 | 2 | 5 |
| **73** | **2.753** | **−8** | **2** | **3** | 7 | 1.923 | 3 | 0 | 14 | 3 | 1.614 | −14 | 3 | 8 |
| **73** | **2.751** | **−4** | **2** | **7** | 9 | 1.913 | 7 | 3 | 7 | 3 | 1.613 | −10 | 3 | 12 |
| 3 | 2.697 | −9 | 1 | 7 | 9 | 1.900 | 9 | 2 | 9 | 3 | 1.612 | 4 | 2 | 15 |
| 2 | 2.637 | 11 | 1 | 1 | 2 | 1.872 | 15 | 1 | 4 | 2 | 1.610 | 7 | 4 | 7 |
| 24 | 2.629 | 7 | 1 | 7 | 2 | 1.868 | 3 | 1 | 14 | 5 | 1.552 | −16 | 3 | 6 |

poorly known. Most of the samples available for the present study represent a single 'M-sartorite' species. An exception is the polished section with two M-sartorites shown in Fig. 7a, with untwinned heptasartorite clearly replacing the twinned enneasartorite, starting from the aggregate periphery. The least twinned portions of the enneasartorite are the best resisting ones to the replacement. In other cases, M-sartorite can overgrow and replace baumhauerite and rathite aggregates (Fig. 7b–d). Further examples show that M-sartorites replace practically all other sartorite homologues present in the deposit. In the majority of such occurrences, M-sartorite is optically untwinned, although in some cases (Fig. 7c), it is polysynthetically twinned.

## 8. Relation to other species

Berlepsch *et al.* (2003) described the complex history of the mineral named 'sartorite', including its chemistry, crystal structure and crystal-chemistry as recalled in the introduction. As already mentioned, 'sartorite' gave the name to a homologous series (Makovicky, 1985, 1997) with two known slab types based on the SnS archetype ($N=3$ and $N=4$, representing the number of polyhedra across each of them). The variety of species is created by combinations of these two unit homologue slabs (*i.e.*, $N_{1-2}=3,4=3.5$) in different ratios (Makovicky, 1985, 1997) and by details of chemical composition. Until the present study, the following minerals had been described (crystal-structure references given): nine-fold sartorite (Berlepsch *et al.*, 2003), guettardite (Makovicky *et al.*, 2012) and twinnite (Makovicky & Topa, 2012) for $N=3$; baumhauerite (Engel & Nowacki, 1970; Topa & Makovicky, 2016), argentobaumhauerite (Topa & Makovicky, 2016) and boscardinite (Orlandi *et al.*, 2012) for $N=3.5$; liveingite (Engel & Nowacki, 1970) for $N=3.67$ (*i.e.*, $N_{1-6}=4,3,4,4,3,4$); dufrénoysite (Ribar *et al.*, 1969), rathite (Berlepsch *et al.*, 2002), polloneite (Topa *et al.*, 2017), veenite (Topa & Makovicky, 2017), carducciite (Biagioni *et al.*, 2014), philrothite (Bindi *et al.*, 2014) and barikaite (Topa *et al.*, 2013) for $N=4$.

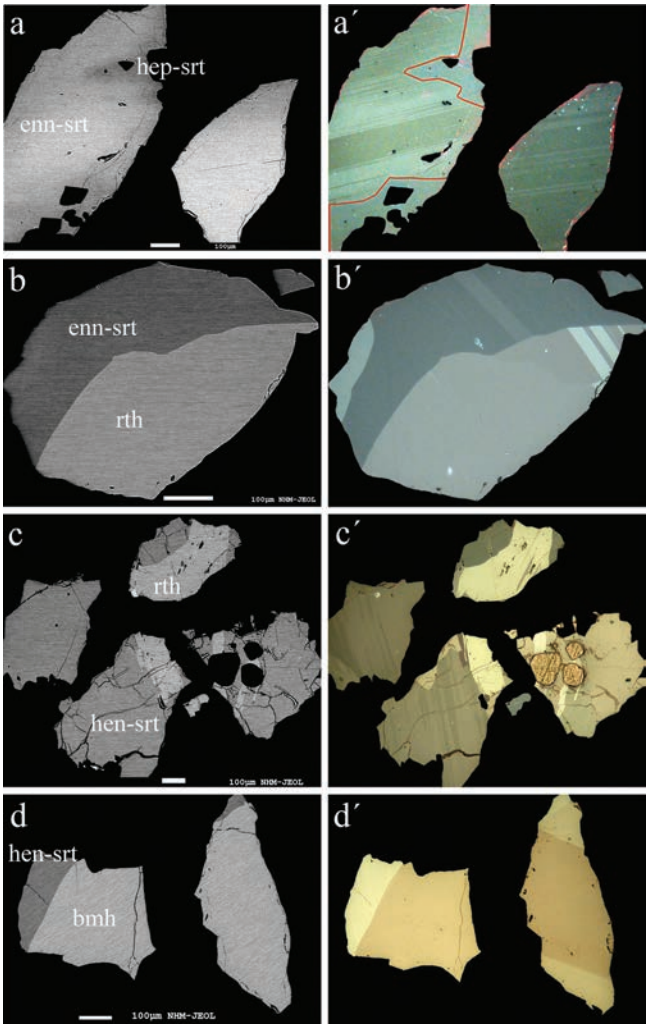


Fig. 7. Backscattered-electron and reflected-light (crossed polarizers) images of hepta-, ennea- and hendekasartorite aggregates from Lengenbach, Binntal, Switzerland. Abbreviations: *bmh* – baumhauerite, *rth* – rathite, *hep-srt* – heptasartorite, *enn-srt* – enneasartorite, *hen-srt* – hendekasartorite. The replacements illustrated in figures *a–d* are described in the text. In *a*, heptasartorite is the phase that constitutes the right-hand margin of the large grain. Scale bar is for 100 μm.

Hepta-, ennea- and hendekasartorite species belong to the lowermost members of the sartorite homologous series (all slabs with $N=3$). For guettardite and twinnite, both being sartorite homologues with $N=3$, antimony plays an important role in chemistry and crystal chemistry, resulting in the 'superperiod' reduced to only $2 \times 4.2$ Å. In 'M-sartorites', antimony does not exceed 1–2 wt%. Silver is absent in them, in agreement with $N=3$.

## 9. Conclusions

The growing amount and quality of data on the old and new phases in the sartorite homologous series illustrate the true nature of covalent compounds with complex coordinations and valencies, present as complications of the basic structural principles of these series. Although the combinatorial character is partly present in other accretional homologous series, here it is the basis of the series, and the anion-omission principle is almost unique among complex sulfides.

On the other hand, with some reservations due to paucity of relevant research material, this study points to a repeated-episodic character of sulfide–sulfosalt mineralization at Lengenbach (Binntal, Switzerland), with M-sartorites as some of the latest sulfosalt minerals, overgrowing but especially replacing the earlier phases. Instead of being a solid solution series, as its linear distribution of phases might suggest, the sartorite anion-omission series is a family of distinct structures and mineral species.

**Acknowledgements:** The authors express their gratitude to all the above listed donors, who contributed material to this study. They also thank Goran Batic for his technical assistance. The paper was handled by Chief Editor S. Krivovichev and the comments and suggestions of two anonymous reviewers helped to improve the manuscript.

## References

Bannister, E.A., Pabst, A., Vaux, G. (1939): The crystallography of sartorite. *Mineral. Mag.*, **25**, 264–270.

Berlepsch, P., Armbruster, T., Topa, D. (2002): Structural and chemical variations in rathite, $Pb_8Pb_{4-x}(Tl_2As_2)_x(Ag_2As_2)As_{16}S_{40}$: modulations of a parent structure. *Z. Kristallogr.*, **217**, 1–10.

Berlepsch, P., Armbruster, T., Makovicky, E., Topa, D. (2003): Another step toward understanding the true nature of sartorite: Determination and refinement of a nine-fold superstructure. *Am. Mineral.*, **88**, 450–461.

Berry, L.G. (1940): Baumahuerite, rathite and sartorite. *in* "Roentgenographic observations on ore minerals". M.A. Peacock, L.G. Berry, eds. University of Toronto Studies. *Geol. Ser.*, **44**, 47–69.

Biagioni, C., Orlandi, P., Moëlo, Y., Bindi, L. (2014): Lead-antimony sulfosalts from Tuscany, (Italy). XVI. Carducciite, $(AgSb)Pb_6(As,Sb)_8S_{20}$, a new Sb-rich isotype of rathite from the Pollone mine, Valdicastello Carducci: occurrence and crystal structure. *Mineral. Mag.*, **78**, 1775–1793.

Biagioni, C., Bindi, L., Nestola, F., Cannon, R., Roth, P., Raber, T. (2016): Ferrostalderite, $CuFe_2TlAs_2S_6$, a new mineral from Lengenbach, Switzerland: occurrence, crystal structure, and emphasis on the role of iron in sulfosalts.*Mineral. Mag.*, **80**, 175–186.

Bindi, L., Nestola, F., Makovicky, E., Guastoni, A., de Battisti, L. (2014): Tl-bearing sulfosalt from the Lengenbach quarry, Binn valley, Switzerland: Philrothite, $TlAs_3S_5$. *Mineral. Mag.*, **78**, 1–9.

Bindi, L., Biagioni, C., Raber, T., Roth, P., Nestola, F. (2015): Ralphcannonite, $AgZn_2TlAs_2S_6$, a new mineral of the routhierite isotypic series from Lengenbach, Binn Valley, Switzerland. *Mineral. Mag.*, **79**, 1089–1098.

Engel, P. & Nowacki, W. (1970): Die Kristallstruktur von Rathit-II. *Z. Kristallogr.*, **131**, 356–375.

Graeser, S., Cannon, R., Drechsler, E., Raber, T., Roth, P. (2008): Faszination Lengenbach. Abbau–Forschung Mineralien 1958–2008. KristalloGrafik Verlag, Lindau, 192 p.

Iitaka, Y. & Nowacki, W. (1961): Refinement of the pseudo crystal structure of scleroclase, $PbAs_2S_4$. *Acta Crystallogr.*, **14**, 1291–1292.

Kraus, W. & Nolze, G. (1999): Powder cell 2.3. Federal Institute for Materials Research and Testing, Berlin.

Laroussi, A., Moëlo, Y., Ohnenstetter, D., Ginderow, D. (1989): Argent et thallium dans les sulfosels de la série de la sartorite (Gisement de Lengenbach, vallée de Binn, Suisse). *C. R. Acad. Sci., Paris*, **308**, 927–933.

Le Bihan, M.-Th. (1962): Étude structurale de quelques sulfures de plomb et d'arsenic naturels du gisement de Binn. *Bull. Soc. Franç. Minéral. Cristallogr.*, **85**, 15–47.

Makovicky, E. (1985): The building principles and classification of sulphosalts based on the SnS archetype. *Fortschr. Mineral.*, **63**, 45–89.

— (1997): Modular crystal chemistry of sulphosalts and other complex sulphides. Chapter 3. *EMU Notes Mineral.*, **1**, 237–271.

Makovicky, E. & Topa, D. (2012): Twinnite, $Pb_{0.8}Tl_{0.1}Sb_{1.3}As_{0.80}S_4$, the OD character and the question of its polytypism. *Z. Kristallogr.*, **227**, 468–475.

—, — (2015): Crystal chemical formula for sartorite homologues. *Mineral. Mag.*, **79**, 25–31.

Makovicky, E., Topa, D., Tajjedin, H., Rastad, E., Yaghubpur, A. (2012): The crystal structure of guettardite, $PbAsSbS_4$. *Can. Mineral.*, **50**, 253–265.

Meisser, N., Roth, P., Nestola, F., Biagioni, C., Bindi, L., Robyr, M. (2017): Richardsollyite, $TlPbAsS_3$, a new sulfosalt from the Lengenbach quarry, Binn Valley, Switzerland. *Eur. J. Mineral.*, **29** (in this issue).

Nowacki, W. & Bahezre, C. (1963): Die Bestimmung der chemischen Zusammensetzung einiger Sulfosalze aus dem Lengenbach (Binnatal, Kt. Wallis) mit Hilfe der elektronischen Mikrosonde. *Schweiz. Mineral. Petrogr. Mitt.*, **43**, 407–411.

Nowacki, W., Iitaka, Y., Buerki, H., Kunz, V. (1961): Structural investigations on sulfosalts from the Lengenbach, Binn Valley (Ct. Wallis). Part II. *Schweiz. Mineral. Petrogr. Mitt.*, **41**, 103–116.

Orlandi, P., Biagioni, C., Bonaccorsi, E., Moëlo, Y., Paar, W.H. (2012): Lead-antimony sulfosalts from Tuscany (Italy). XII. Boscardinite, $TlPb_3(Sb_7As_2)_{\Sigma 9}S_{18}$, a new mineral species from the Monte Arsiccio mine: occurrence and crystal structure. *Can. Mineral.*, **50**, 235–251.

Palache, C., Bermann, H., Frondel, C. (1944): Dana's System of Mineralogy (7th edition). John Wiley & Sons, New York, Vol. 1, 478–480.

Pring, A. (2001): The crystal chemistry of the sartorite group minerals from Lengenbach Binntal, Switzerland – a HRTEM study. *Schweiz. Mineral. Petrogr. Mitt.*, **81**, 69–87.

Pring, A., Williams, T., Withers, R. (1993): Structural modulation in sartorite: an electron microscopy study. *Am. Mineral.*, **78**, 619–626.

Ribar, B., Nicca, C., Nowacki, W. (1969): Dreidimensionale Verfeinerung der Kristallstruktur von Dufrénoysit, $Pb_8As_8S_{20}$. *Z. Kristallogr.*, **130**, 15–40.

Roth, P., Raber, T., Drechsler, E., Cannon, R. (2014): The Lengenbach Quarry, Binn Valley, Switzerland. *Mineral. Rec.*, **45**, 157–196.

Topa, D. & Makovicky, E. (2016): Argentobaumhauerite: name, chemistry, crystal structure, comparison with baumhauerite, and position in the Lengenbach mineralization sequence. *Mineral. Mag.*, **80**, 819–840.

—, — (2017): The crystal structure of veenite. *Mineral. Mag.*, **81**, DOI:10.1180/minmag.2016.080.141.

Topa, D., Makovicky, E., Tajedin, H., Putz, H., Zagler, G. (2013): Barikaite, $Ag_3Pb_{10}(Sb_8As_{11})_{\Sigma 19}S_{40}$, a new member of the sartorite homologous series. *Mineral. Mag.*, **77**, 3039–3046.

Topa, D., Graeser, S., Makovicky, E., Stanley, C. (2016a): Argentoliveingite, IMA 2016-029. CNMNC Newsletter No. 32, October 2016, p. 920. *Mineral. Mag.*, **80**, 915–922.

Topa, D., Makovicky, E., Stanley, C., Cannon, R. (2016b): Argentodufrénoysite, IMA 2016-046. CNMNC Newsletter No. 33, October 2016, p. 1138. *Mineral. Mag.*, **80**, 1135–1144.

Topa, D., Keutsch, F., Makovicky, E., Kolitsch, U., Paar, H.W. (2017): Polloneite, a new complex Pb(–Ag)–As–Sb sulfosalt from the Pollone mine, Apuan Alps, Tuscany, Italy. *Mineral. Mag.*, **81**, DOI:10.1180/minmag.2017.081.003.

vom Rath, G. (1864): Mineralogische Mitteilungen. *Ann. Phys. Chem.*, **122**, 371–399.

*Received 26 October 2016*
*Modified version received 8 December 2016*
*Accepted 13 February 2017*